Energy resolution and efficiency studies for the backward end cap calorimeter of P̄ANDA

María Carmen Mora Espí*and Dmitry Khaneft

Contents

*Corresponding author: moraespi@kph.uni-mainz.de

1 Motivation

1.1 The panda experiment

P̄ANDA is a new detector that will be build at GSI belonging to the new FAIR facilities. Its characteristics and geometry will give access to study several processes. In our case we are mainly interested in the structure of the nucleon. With P̄ANDA properties we will be able to measure the Form Factors of the proton (FF) in time-like region up to a momentum transferred of $Q^2 = 14\,\mathrm{GeV}^2$ (see [1]).

The FFs have been measured several times in different experimets in the so called space-like region. There all data are consistent and no controversies can be found while for the time-like region only few experiments have reached a good count rate and therefore good statistics. Morover the results of these measurements, calculated by using different techniques, are in disagreement with each other.

Apart of all this, there is a physical threshold determined by the proton mass. Up to now no data have been taken under these threshold so that there is a region between $0\,(\mathrm{GeV/c})^2$ and $4\mathrm{m}_p^2$ in which there is no data. One possibility to scan the unphysical region would be to use the reaction $\bar{p}p \rightarrow e^+e^-\pi^0$ in that cases in wich the momentum transferred to the electron-positron pair is below the threshold.

To be able to measure the final products of this reaction one will need a very good efficiency and energy resolution, specially at very forward and backward angles. Therefore the simulation study have been done including also the additional

dead material which represents the cabling ans supplies of the STT and MVD detectors.

2 Simulation and analysis

2.0.1 Simulation

For studying the Energy resolution and efficiency of the backward end cap calorimeter, several steps have been followed.

(1) Dead material for STT
The first simulation was done without including dead material representing the cabling and supplies of other subdetectors. Then a disc of Aluminum 2 cm thick was included behind the STT detector to represent its cabling and readout electronics. Another simulation with a disc 4 cm thick was later done.

(2) Dead material for MVD
After this first studies, the dead material that supplies and cabling for MVD detector was estimated and a representation of it was implemented for the simulation. Together with MVD dead material was included also the intermediate case for the SST representative dead material.

(3 and 4) Complete Map of EMC
Later a third simulation covering half quarter of the calorimeter in θ (from... to...) and ϕ(from... to...) angles and the energy ranges for particles expected at backward end cap was done. This simulation was done in two steps, first only for 250 MeV photons, five θ angles and six ϕ angles for which one have 30 points to measure the efficiency and energy resolution. Last it was done for 10 θ and ϕ angles, covering the half quarter with 100 diferent points which already gives a good idea of the behaviour of the whole detector.

All simulations have been done with 50.000 monoenergetic photons covering the energy range expected for the particles hiting the backward end cap calorimeter.

One can see in table 1 the simulations characteristics for each case.

Case	Energy (MeV)	θ	ϕ	Dead Material Stt	Dead Material MVD
1	30 100 250 500 700	145 150 155 160 165	1 22.5 45	None 2 cm Al 4 cm Al	None
2a	30 250 700	147.5	78	2 cm Al	Estimation
2b	30 250 700	152.5	34.5	2 cm Al	Estimation
2c	30 250 700	152.5	45	2 cm Al	Estimation
3	250	151 154 157 160 163	314 323 332 341 350 359	2 cm Al	Estimation
4	30 100 250 500 700	150 151.5 153 154.5 156 157.5 159 160.5 162 163.5	314 319 324 329 334 339 344 349 354 359	2 cm Al	Estimation

Table 1: Characteristics of each simulation

2.0.2 Analysis

Signal from background separation was proved but without relevant results.

For the analysis only the bump with highest energy was selected per event and the resulting energy histogram was fitted using the novosibirsk function plus a constant.

$$f(E) = A\exp\left\{-\frac{1}{2}\left[\frac{\ln^2\left[1+\Lambda\tau(E-E_0)\right]}{\tau^2}+\tau^2\right]\right\}$$

with

$$\Lambda = \frac{\sinh\left(\tau\sqrt{\ln(4)}\right)}{\sigma\tau\sqrt{ln(4)}}$$

The full width at half maximum (FWHM) is defined in this function as

$$FWHM = 2.35\sigma$$

In this formula, E_0 represents the peak position, σ is the width and τ is the so called tail parameter that gives us an idea of the distortion of the peak. It has been checked that the fit using a novosibirsk function plus a constant gives in general better χ^2 values. The fit ranges have been choosen also to improve the value of the χ^2

For the calculation of the energy resolution has been taken into account the FWHM, defining the energy resolution as follows

$$E_{res} = 2\sigma\frac{\sqrt{\ln 4}}{E_0}$$

being σ and E_0 the values extacted from fit parameters.

The integral of the fit function from $\mu - 3\sigma$ until $\mu + 2\sigma$ has been calculated and divided by 50.000 (the generated number of events) to calculate the efficiency in each case.

$$Eff = \frac{1}{50000}\int_{\mu-3\sigma}^{\mu+2\sigma} f(E)dE$$

Using again the values for μ and σ extracted from the fit parameters.

3 Results

3.0.3 Dead material for STT

Figure 1 represents squematichaly how are the trajectories for different θ angles for the cases $\phi = 1°$, $\phi = 22.5°$and $\phi = 45°$,

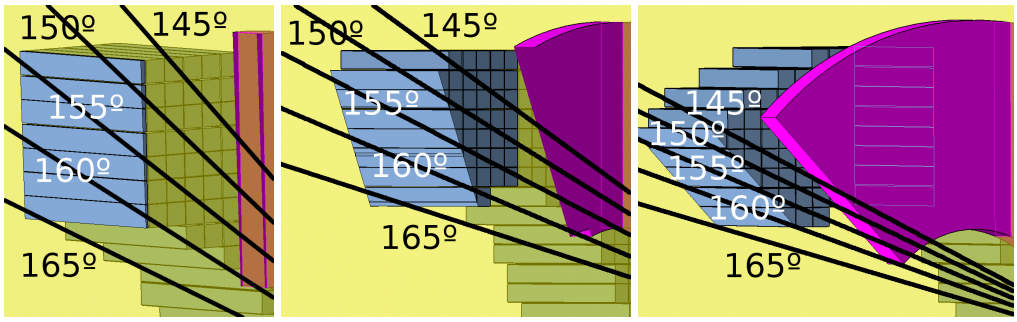

$\phi = 1°$ $\phi = 22.5°$ $\phi = 45°$

Figure 1: Detail of the trajectories of the generated photons in respect to the backward calorimeter for different ϕ angles.

As one can see from these pictures the photons generated in the simulations done at $\theta = 145°$do not hit the calorimeter, so we do not reconstruct a good Energy peak, our particles are lost and only some signal comming from sencondary particles (electron-positron pairs or bremstrahlung photons) are detected. A typical histogram for this case can be seen in figure 2

Photons that have been generated at $\theta = 150°$reach the calorimeter, but the electromagnetic shower is not fully contained inside the crystals, so we loose some information about the energy of the particles. A typical energy histogram is represented in figure 3. The width of the peak is a bit bigger than expected.

A typical histogram for the cases in which the photons reach the calorimeter in a good angle and the shower is developed fully inside can be seen in figure 4

The rough results of this first analysis done to have an idea of our efficiencies and energie resolutions are summarized in table 2. For more specific results look into the appendix for Tables 3, 4, 5, 6, 7.

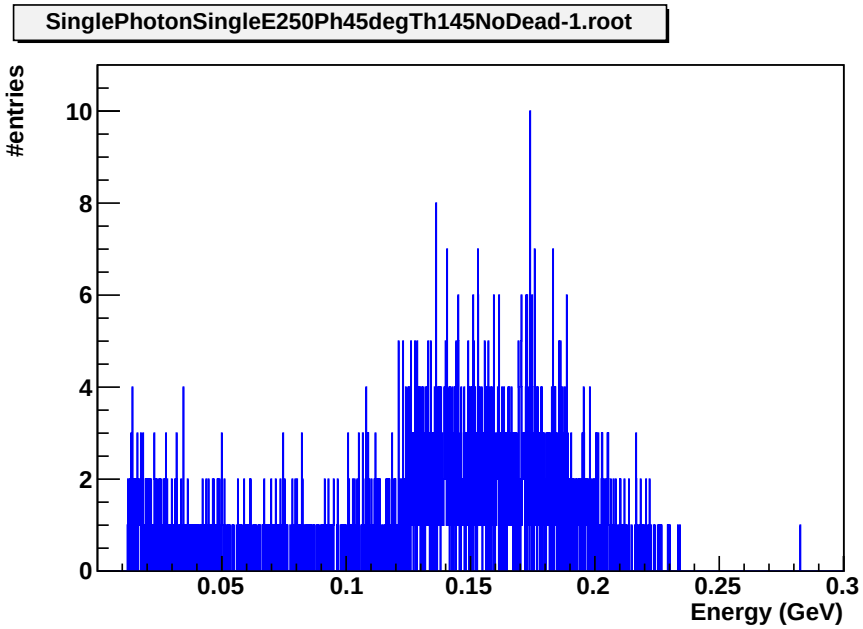

Figure 2: Typical histogram for simulations with $\theta = 145°$. This particular case corresponds to E=250 MeV and ϕ=45°.

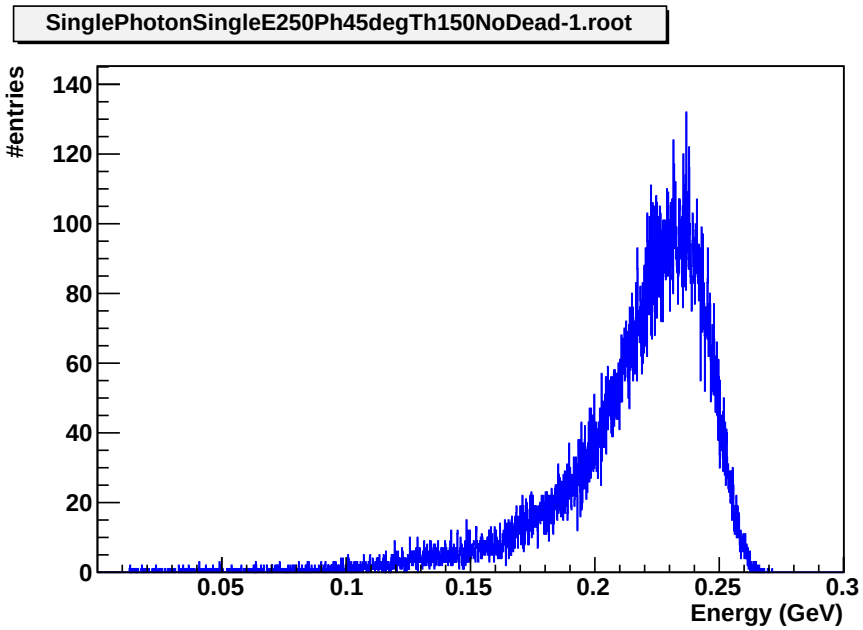

Figure 3: Typical histogram for simulations with $\theta = 150°$. This particular case corresponds to E=250 MeV and ϕ=45°.

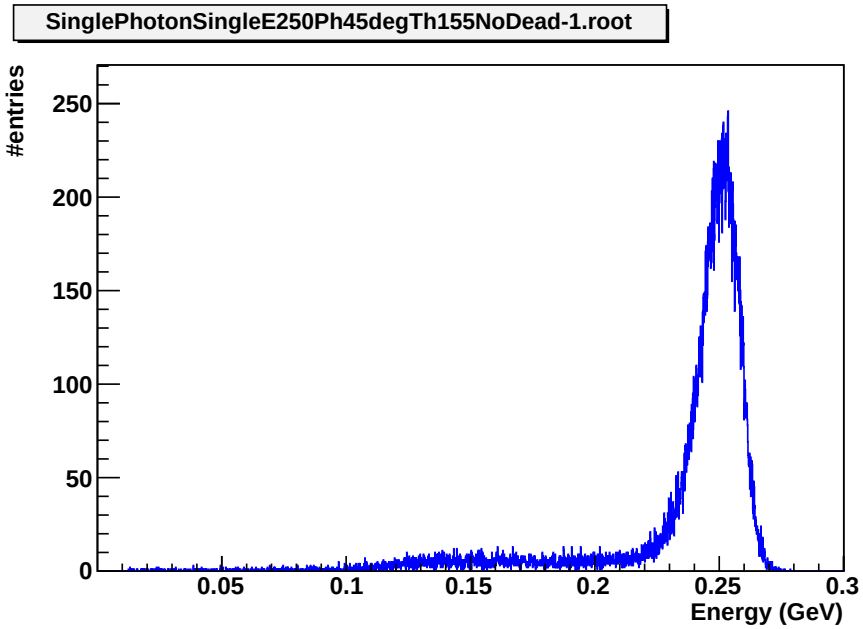

Figure 4: Typical histogram for simulations at angles fully inside the calorimeter. This particular case is at E=250 MeV, $\theta = 155°$and ϕ=45°.

Energy	Efficiency	R_E	Estimated R_E
30 MeV	70%	25%	24%
100 MeV	66%	13%	16%
250 MeV	65%	7%	9%
500 MeV	67%	5%	7%
700 MeV	70%	4%	6%

Table 2: Rough results of first simulation done with single photons at diferent energies and θ and ϕ angles. For wich cases of dead material?

3.0.4 MVD

The backward end cap calorimeter is placed at approximately $\theta \in]145^o, 165^o[$ where the maximum amount of dead material is introduced by the MVD electronics and supporting system. An estimation of this geometry has been done based on the dead material calculation represented in figure 5. The estimated geometry according to these values can be seen in figure 6 but for simplification, just cubes were used for the first analysis. This geometry can be seen in figure 7.

The first study of the efect of the dead material introduced by the electronics

introducir algo más de cómo se ha hecho la estimación y que materiales se han utilizado para

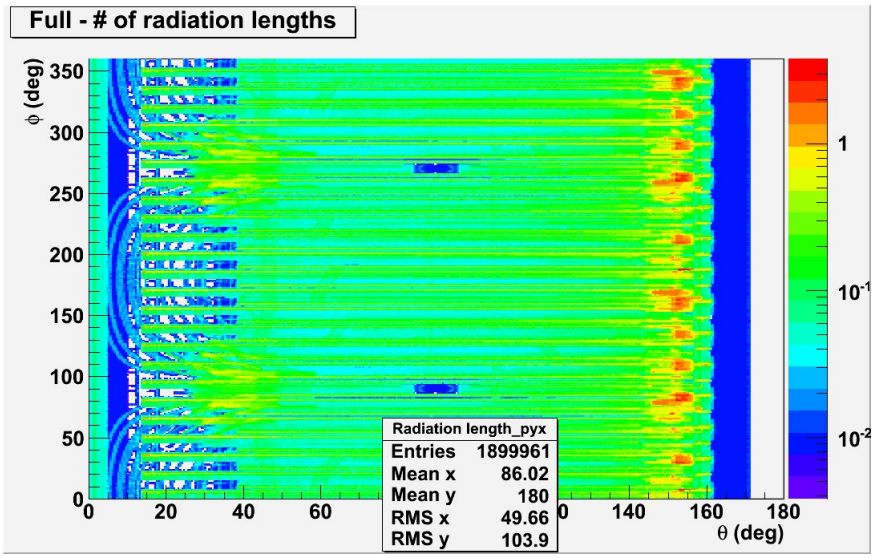

Figure 5: Plot representing the dead material introduced by several subdetectors of $\bar{\text{P}}$ANDA [5]. The backward end cap calorimeter is placed at approximately $\theta \in]145^{o}, 165^{o}[$ where the maximum amount of dead material is introduced by the MVD electronics and supporting system. An estimation of this geometry has been done based on this plot.

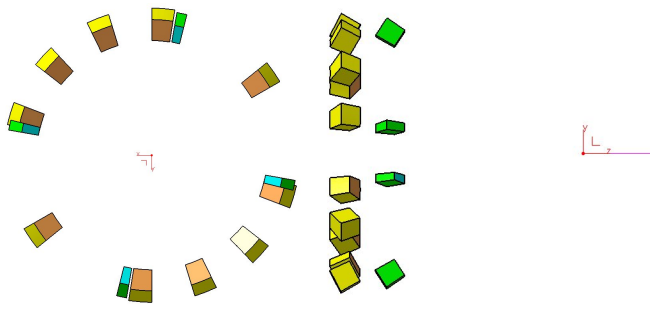

Figure 6: Estimated geometry of the dead material introduced by the electronics and support system of the MVD in front of the EMC. Based on figure 5.

of MVD has been done only at three energies (30 MeV, 250 MeV and 700 MeV) and three combinations of θ and ϕ angles. The angles θ and ϕ have been choosen so that the small block of dead material of MVD was hit, the big block was hit and none was hit. This corresponds to $\theta = 147.5°$and $\phi = 78°$(figure 8), $\theta = 152.5°$and $\phi = 34.5°$(figure 9) and $\theta = 152.5°$and $\phi = 45°$(figure 10) respectively.

As one can also see in figure 8, the photons generated at θ=147°do not hit

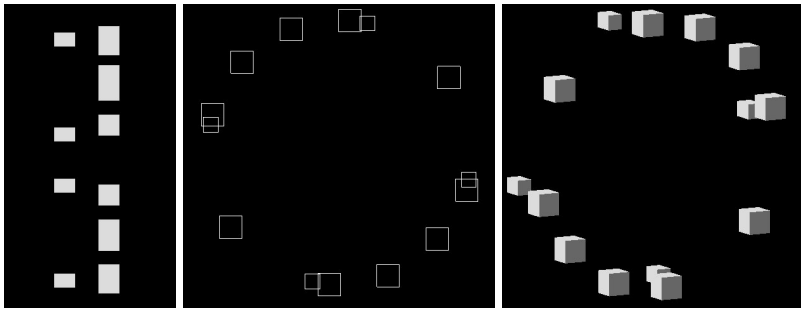

Figure 7: Simplified geometry of the estimation seen in figure 6 used for the simulation of the dead material introduced by the cabling and support systems of the MVD.

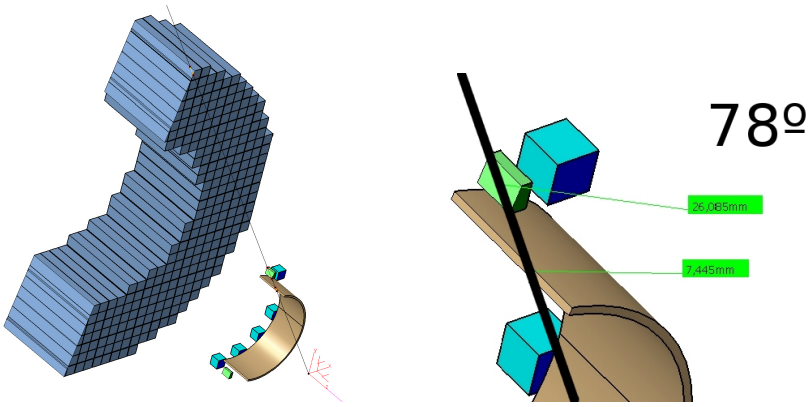

Figure 8: $\theta = 147.5°$, $\phi = 78°$, E= 30 MeV, 250 MeV and 700 MeV; X_0 Cu = 14.3 mm: 26.085 mm$\rightarrow$ 1.82 X_0; 7.445 mm$\rightarrow$ 0.52 X_0

completely the calorimeter, so one expect bad reconstruction of this peak. The third column in figure 11 corresponds to this angular cases for 30 MeV, 250 MeV and 700 MeV respectively from top to bottom. Only in the first case a very small peak can be seen because the cross section of photons at 30 MeV is very small inside the material .

meter un plot de la cross section de fotones????

The efficiency and energy resolution calculated as explained before show still acceptable results for our purposes. Efficiency is very much lowered in the cases in wich we have more dead material but the energy resolution is almost not affected by introduction of more material in front of the calorimeter. The exact values can be read in figure 12

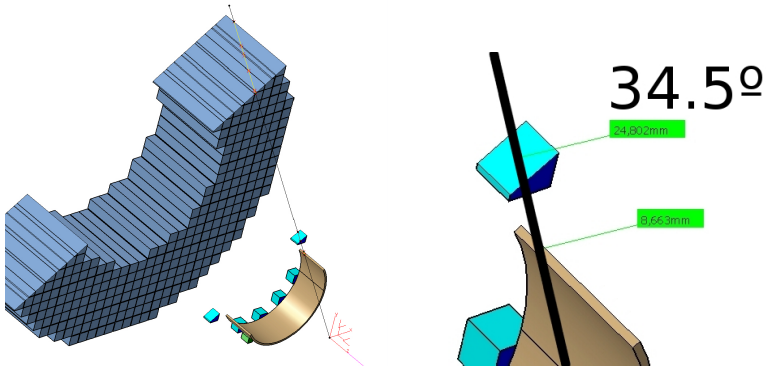

Figure 9: $\theta = 152.5°$, $\phi = 34.5°$, E= 30 MeV, 250 MeV and 700 MeV; X_0 Cu = 14.3 mm: 24.802 mm→ 1.73 X_0; 8.663 mm→ 0.61 X_0

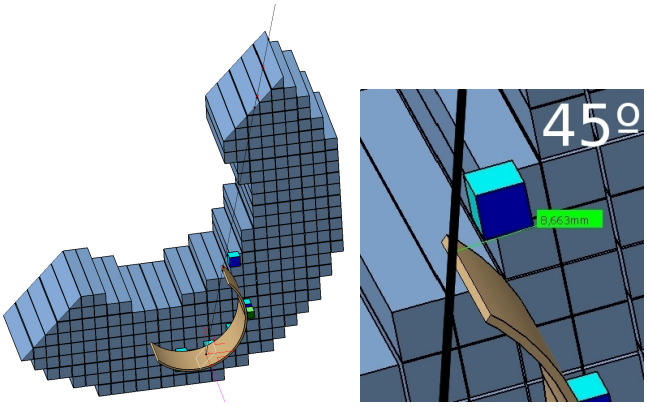

Figure 10: $\theta = 152.5°$, $\phi = 45°$, E= 30 MeV, 250 MeV and 700 MeV; X_0 Cu = 14.3 mm: 8.663 mm→ 0.61 X_0

3.0.5 Mapping

The reults of the simulation number 3 (see table 1) are not presented here because all of them are also included in the results of simulation number 4 (table 1).

In this last case 100 different combinations of θ and ϕ (10 θ angles and 10 ϕ angles) were choosen for the simulations covering half quarter of the calorimeter (for symmetry reasons). In total five different energies have been selected to cover

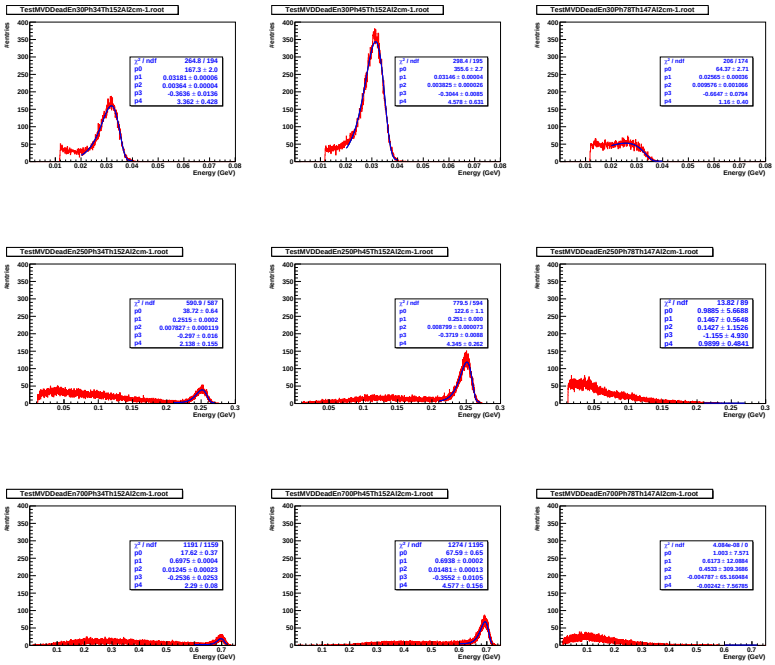

Figure 11: MVD dead material studies results Plots for histograms.

the expected ranges of energies expected at the backward end cap calorimeter.

In figures 33, 34, 35, 36 and 37 one can see the histograms and the fits used for the analysis for the different energies.

Figures 38, 39, 40, 41 and 42 show the results obtained for the Efficiency and energy resolutions at each energy. The results are still inside our limits. In the efficiency histograms one can observe where a block of dead material is found by the generated photons as well as the influence of the Alumninum plate used for simulate the electronics of STT.

The efficiency and energy resolution is then satisfactory for our measurements.

4 Comparison with pandaroot

Something to say here?...

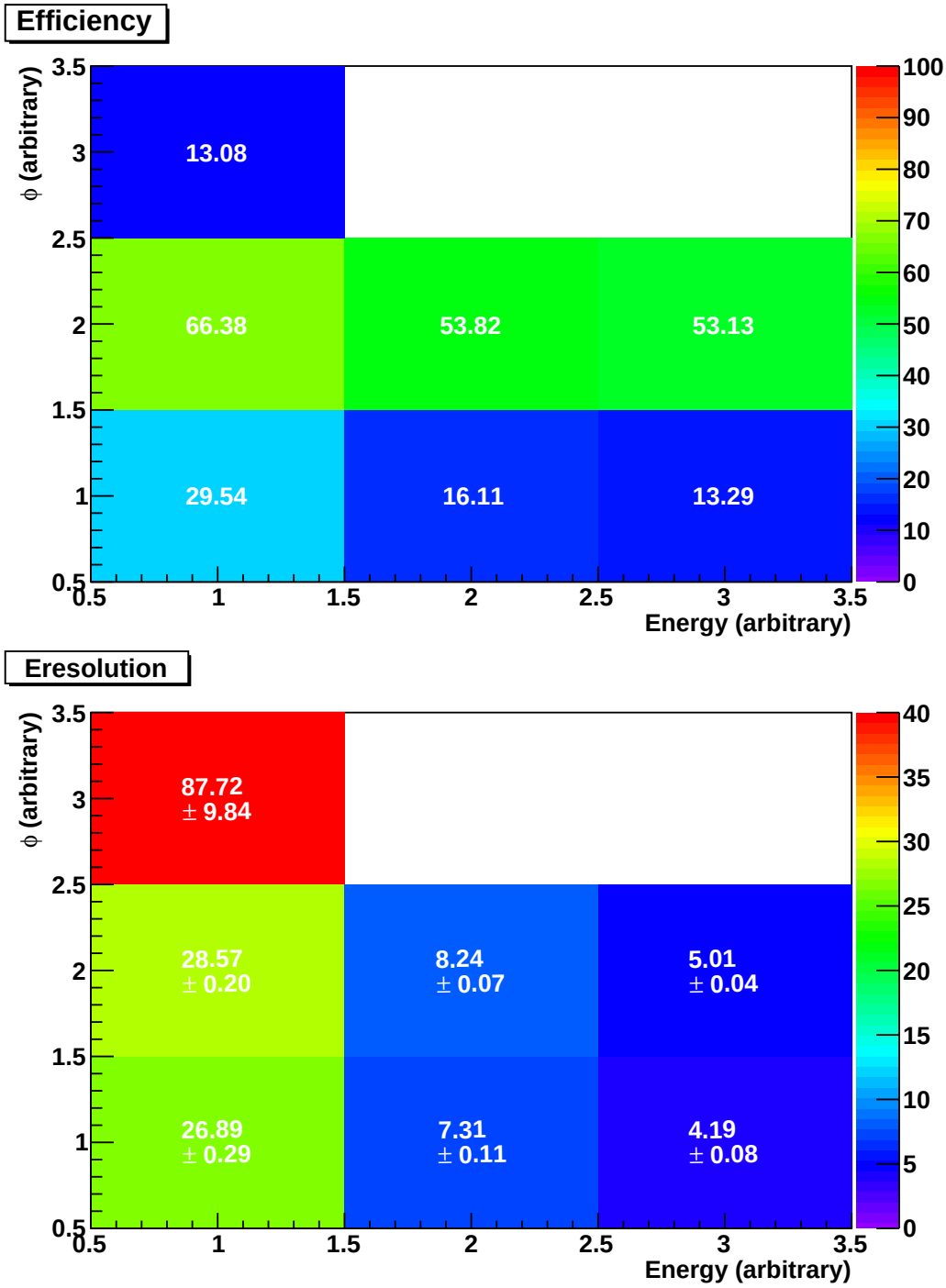

Figure 12: Efficiency and energy resolution including MVD dead material. Labels: ϕ: 1→?, 2→?, 3→?; Energy: 1→30 MeV, 2→250 MeV, 3→700 MeV.

5 Conclusions

The results are the following:

6 Appendix

6.1 First simulation

6.1.1 Tables

			30 MeV		
			150°	**155°**	**160°**
0 cm Al	**45°**	Efficiency	90.78	84.58	82.29
		E_{res}	28.72±0.16	26.21±0.14	23.51±0.13
	22.5°	Efficiency	89.56	84.28	82.47
		E_{res}	27.57±0.15	23.32±0.12	23.38±0.13
	1°	Efficiency	87.6	84.53	82.24
		E_{res}	29.21±0.17	24.29±0.13	25.15±0.15
			150°	**155°**	**160°**
2 cm Al	**45°**	Efficiency	85.6	77.74	77.4
		E_{res}	31.54±0.20	27.67±0.17	23.56±0.13
	22.5°	Efficiency	83.83	77.72	77.56
		E_{res}	29.91±0.18	24.33±0.16	23.56±0.13
	1°	Efficiency	82.97	77.23	77.4
		E_{res}	31.96±0.21	25.37±0.15	25.25±0.16
			150°	**155°**	**160°**
4 cm Al	**45°**	Efficiency	75.17	69.23	68.71
		E_{res}	31.54±0.20	27.67±0.17	23.56±0.13
	22.5°	Efficiency	73.32	68.83	69.02
		E_{res}	29.91±0.18	24.33±0.16	23.56±0.13
	1°	Efficiency	73.15	69.08	66.47
		E_{res}	31.96±0.21	25.37±0.15	25.25±0.16

Table 3: Results for 30 MeV. Includes the study of the dead material of STT. No dead material for MVD is included yet

			100 MeV		
			150°	**155°**	**160°**
0 cm Al	**45°**	Efficiency	88.07	84.83	82.02
		E_{res}	20.26±0.11	12.60±0.06	12.57±0.06
	22.5°	Efficiency	85.58	84.52	82.28
		E_{res}	19.87±0.12	12.20±0.06	12.28±0.06
	1°	Efficiency	84.48	84.57	82.28
		E_{res}	23.51±0.15	12.28±0.06	12.55±0.06
			150°	**155°**	**160°**
2 cm Al	**45°**	Efficiency	72.77	74.91	77.73
		E_{res}	20.82±0.18	13.02±0.07	12.82±0.07
	22.5°	Efficiency	71.21	74.68	77.46
		E_{res}	20.19±0.19	12.63±0.07	12.41±0.06
	1°	Efficiency	64.64	74.78	77.77
		E_{res}	23.88±0.30	12.71±0.07	12.68±0.07
			150°	**155°**	**160°**
4 cm Al	**45°**	Efficiency	62.69	65.23	68.25
		E_{res}	20.73±0.21	13.23±0.08	13.09±0.08
	22.5°	Efficiency	61.18	64.78	67.59
		E_{res}	20.92±0.22	12.66±0.08	12.48±0.07
	1°	Efficiency	55.79	65.32	67.54
		E_{res}	24.91±0.39	13.00±0.08	12.82±0.08

Table 4: Results for 100 MeV. Includes the study of the dead material of STT. No dead material for MVD is included yet.

			250 MeV		
			150°	**155°**	**160°**
0 cm Al	**45°**	Efficiency	87.7	84.07	81.99
		E_{res}	18.31±0.12	7.20±0.03	7.39±0.03
	22.5°	Efficiency	85.01	84.06	81.89
		E_{res}	19.86±0.14	7.07±0.03	7.09±0.03
	1°	Efficiency	85.39	84	81.92
		E_{res}	25.24±0.18	6.97±0.03	7.27±0.03
			150°	**155°**	**160°**
2 cm Al	**45°**	Efficiency	81.85	72.97	77.11
		E_{res}	19.94±0.14	7.23±0.04	12.82±0.07
	22.5°	Efficiency	79.57	72.25	76.81
		E_{res}	22.18±0.18	7.04±0.04	7.03±0.04
	1°	Efficiency	73.1	72.26	77
		E_{res}	27.19±0.29	6.91±0.04	7.30±0.04
			150°	**155°**	**160°**
4 cm Al	**45°**	Efficiency	74.83	62.34	67.24
		E_{res}	21.92±0.19	7.20±0.05	7.43±0.05
	22.5°	Efficiency	72.1	61.54	66.94
		E_{res}	25.06±0.25	6.92±0.05	7.12±0.04
	1°	Efficiency	66.67	61.89	66.68
		E_{res}	30.49±0.42	7.04±0.05	7.36±0.05

Table 5: Results for 250 MeV. Includes the study of the dead material of STT. No dead material for MVD is included yet.

			500 MeV		
			150°	**155°**	**160°**
0 cm Al	**45°**	Efficiency	85.18	83.64	82.2
		E_{res}	17.18±0.12	4.83±0.02	4.95±0.02
	22.5°	Efficiency	82.97	83.32	81.81
		E_{res}	20.68±0.17	4.68±0.02	4.78±0.02
	1°	Efficiency	79.61	83.05	82.06
		E_{res}	26.28±0.23	4.74±0.02	5.02±0.02
			150°	**155°**	**160°**
2 cm Al	**45°**	Efficiency	80.2	74.05	78.98
		E_{res}	18.37±0.15	4.97±0.02	5.07±0.02
	22.5°	Efficiency	74.45	73.22	78.13
		E_{res}	22.86±0.25	4.79±0.02	4.89±0.02
	1°	Efficiency	63.51	72.75	78.93
		E_{res}	28.80±0.55	4.85±0.02	5.17±0.03
			150°	**155°**	**160°**
4 cm Al	**45°**	Efficiency	75.57	64.71	71.69
		E_{res}	19.95±0.19	5.18±0.03	5.62±0.04
	22.5°	Efficiency	70.71	63.59	69.49
		E_{res}	24.38±0.30	5.00±0.04	5.25±0.03
	1°	Efficiency	61.25	63.42	70.29
		E_{res}	30.52±0.69	5.00±0.03	5.46±0.03

Table 6: Results for 500 MeV. Includes the study of the dead material of STT. No dead material for MVD is included yet.

			700 MeV		
			150°	**155°**	**160°**
0 cm Al	**45°**	Efficiency	83.4	83.23	82.76
		E_{res}	16.66±0.12	4.01±0.02	4.18±0.02
	22.5°	Efficiency	81.23	82.97	82.1
		E_{res}	21.54±0.20	3.84±0.02	3.97±0.02
	1°	Efficiency	77.59	82.51	82.71
		E_{res}	27.31±0.27	3.88±0.02	4.21±0.02
			150°	**155°**	**160°**
2 cm Al	**45°**	Efficiency	80.18	75.1	80.55
		E_{res}	17.88±0.15	4.22±0.02	4.37±0.02
	22.5°	Efficiency	77.1	73.75	79.43
		E_{res}	22.79±0.23	4.02±0.02	4.17±0.02
	1°	Efficiency	68.6	73.8	79.86
		E_{res}	28.78±0.41	4.07±0.02	4.37±0.02
			150°	**155°**	**160°**
4 cm Al	**45°**	Efficiency	77.89	67.13	73.65
		E_{res}	19.09±0.18	4.64±0.03	4.98±0.03
	22.5°	Efficiency	75.28	66.35	71.94
		E_{res}	23.22±0.24	4.47±0.03	4.63±0.03
	1°	Efficiency	67.47	65.74	73.04
		E_{res}	30.58±0.51	4.39±0.03	4.85±0.03

Table 7: Results for 700 MeV. Includes the study of the dead material of STT. No dead material for MVD is included yet.

6.1.2 Fits

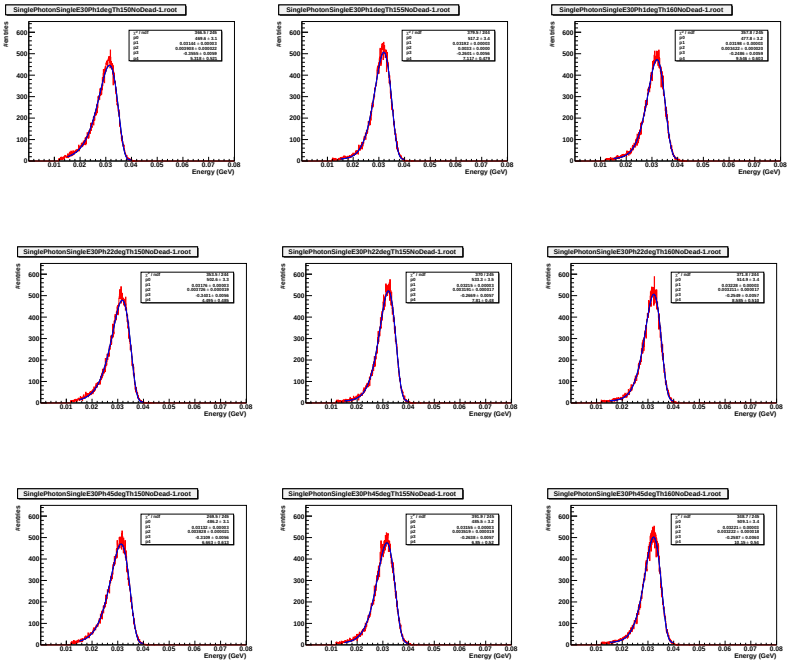

Figure 13: 30 MeV No dead material

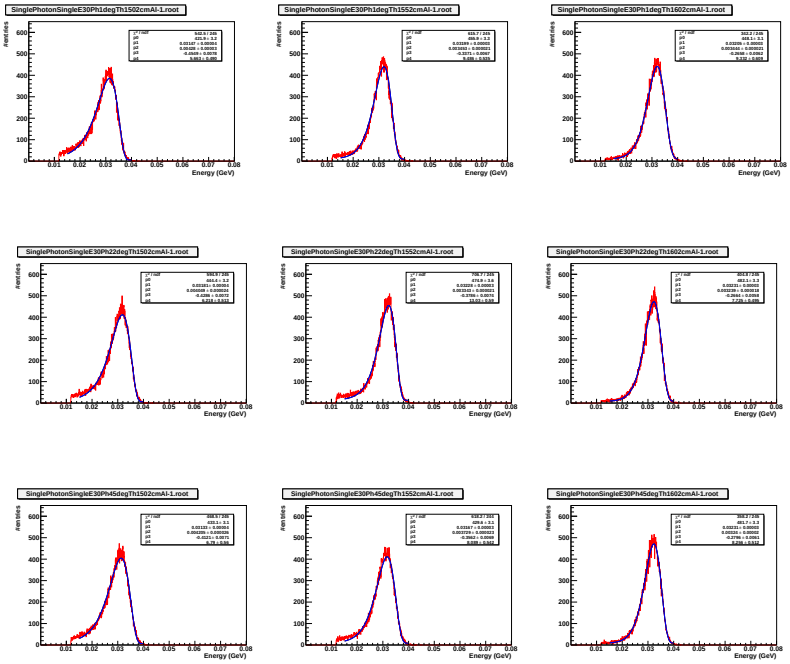

Figure 14: 30 MeV 2 cm Al

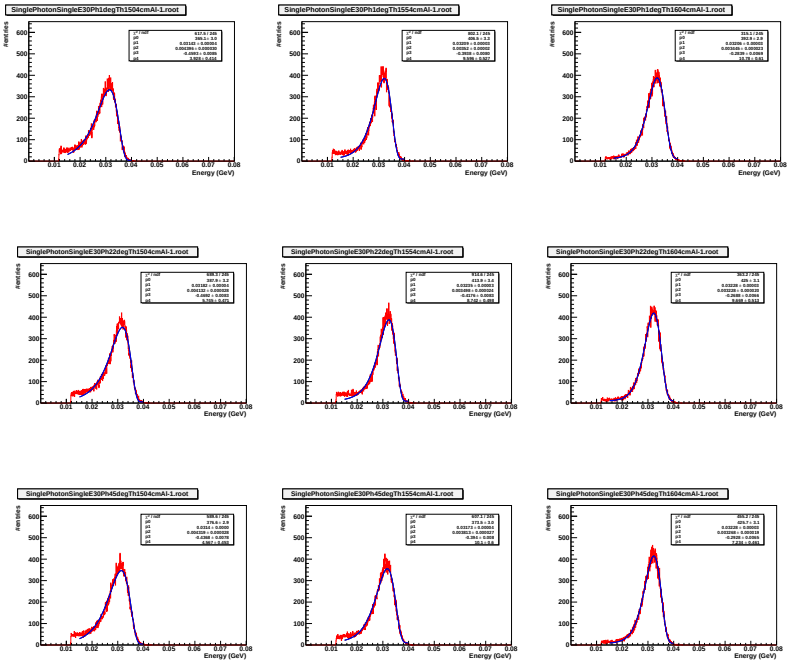

Figure 15: 30 MeV 4 cm Al

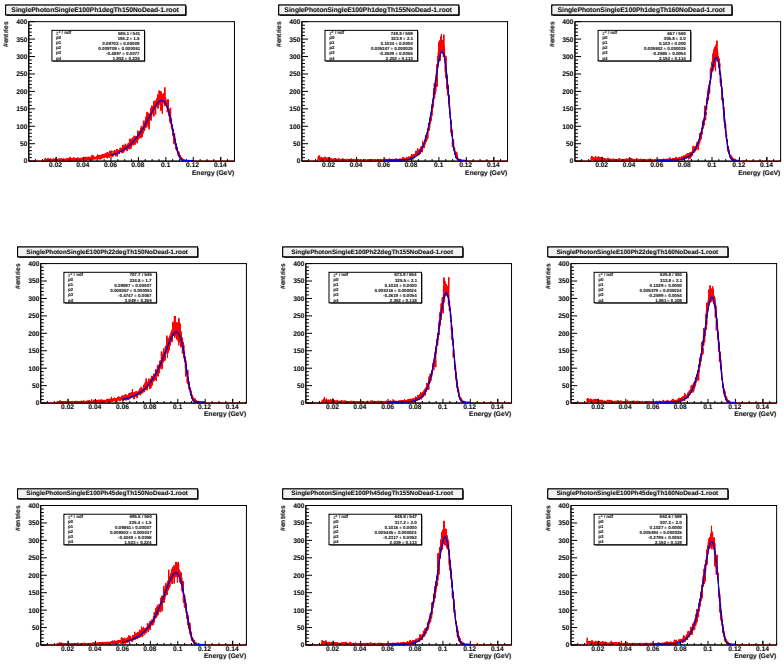

Figure 16: 100 MeV No dead material

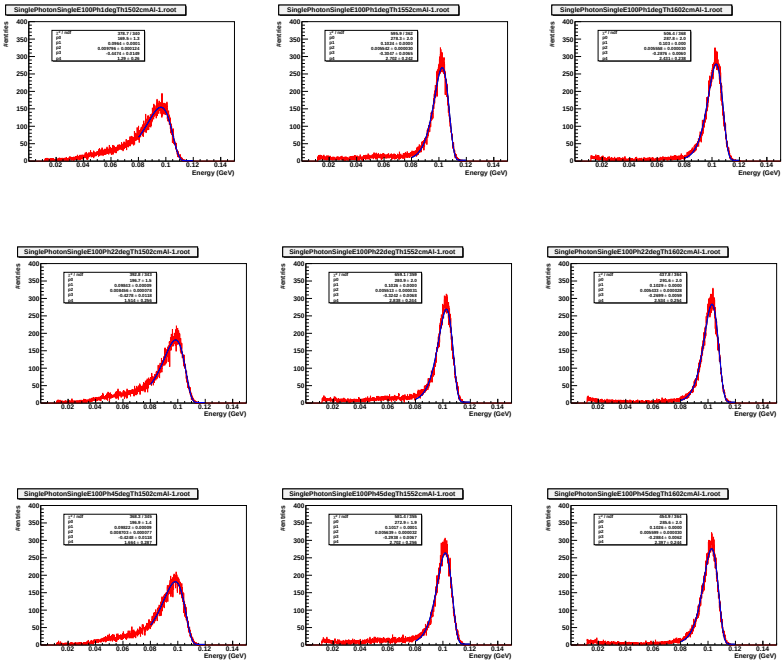

Figure 17: 100 MeV 2 cm Al

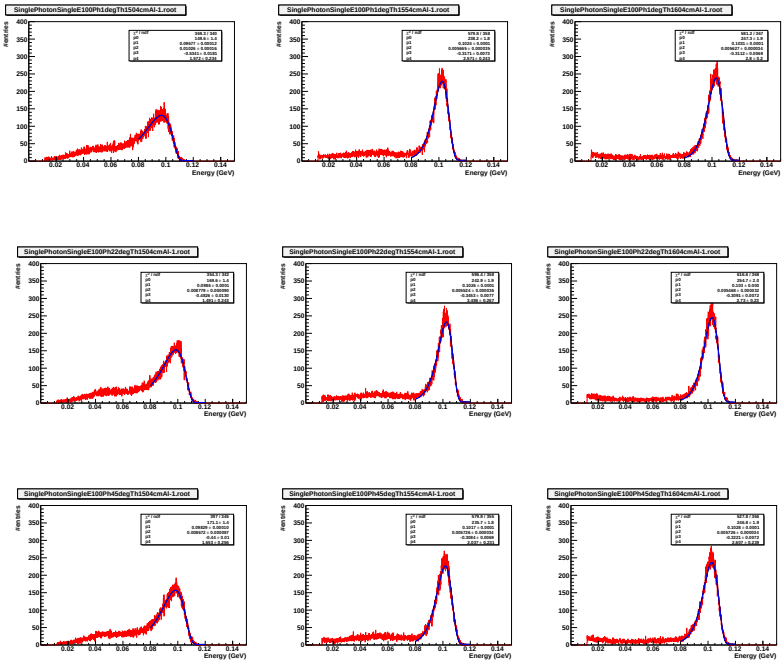

Figure 18: 100 MeV 4 cm Al

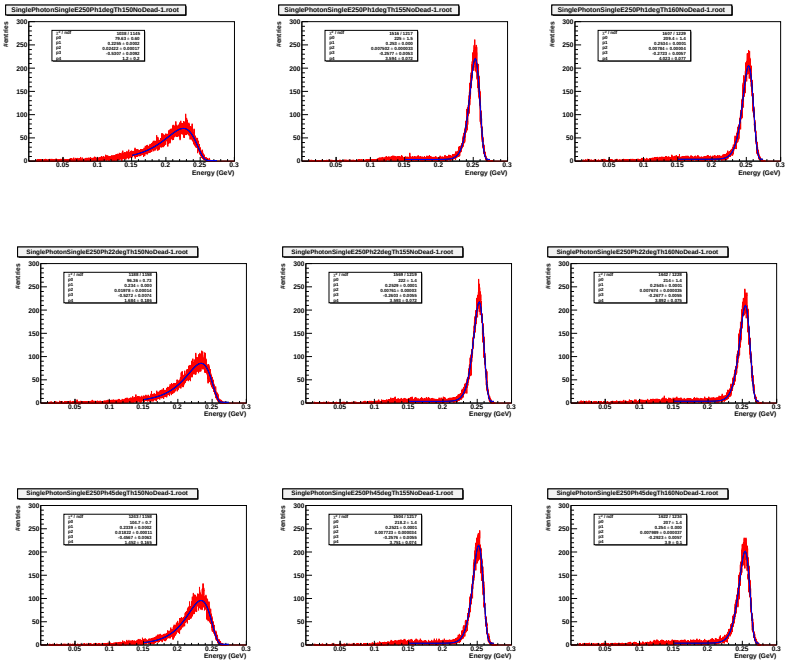

Figure 19: 250 MeV No dead material

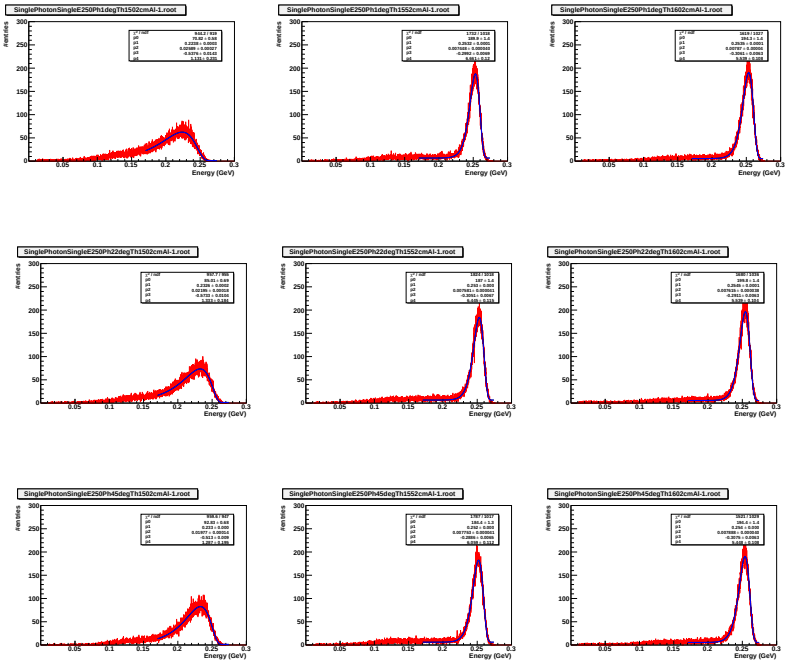

Figure 20: 250 MeV 2 cm Al

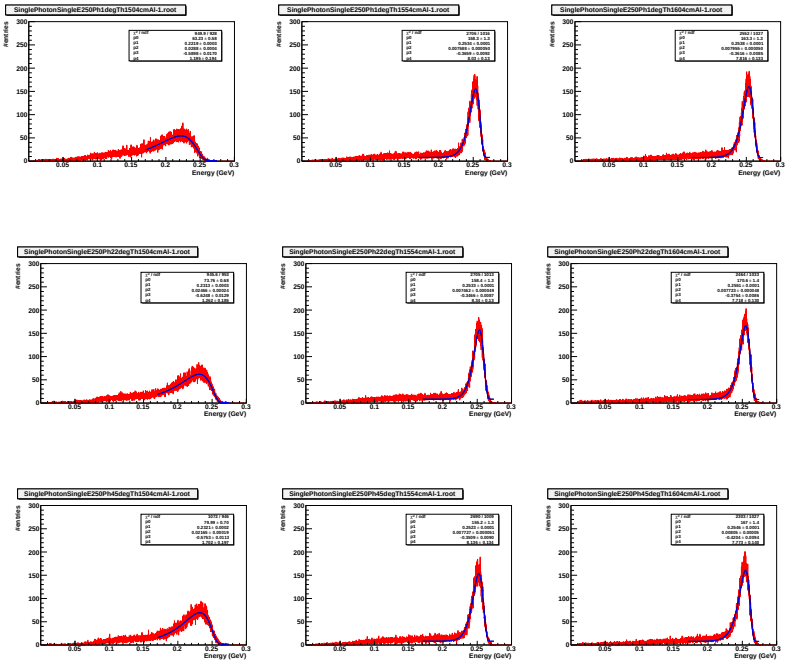

Figure 21: 250 MeV 4 cm Al

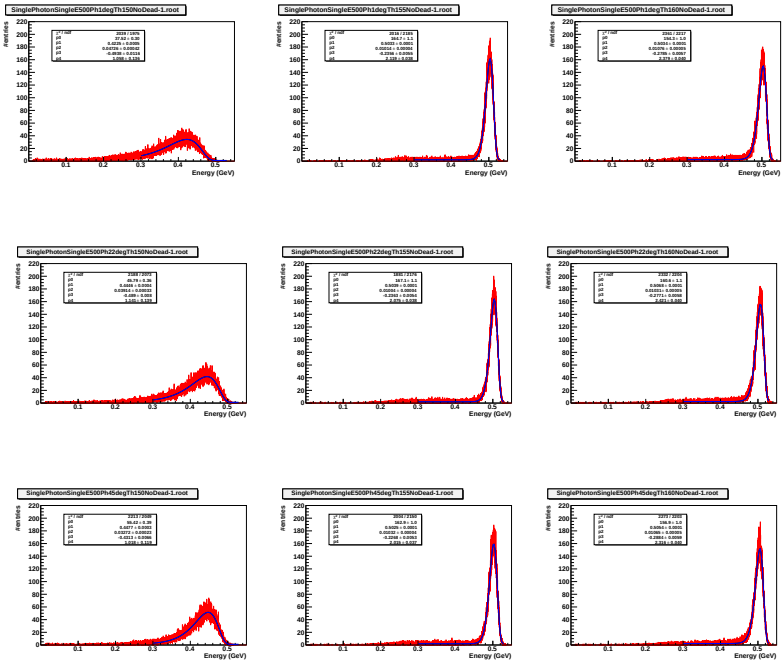

Figure 22: 500 MeV No dead material

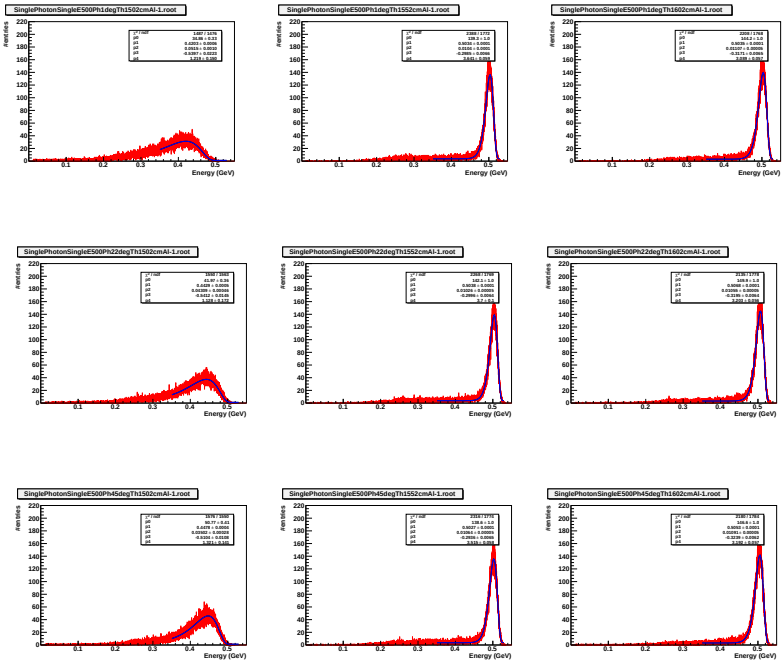

Figure 23: 500 MeV 2 cm Al

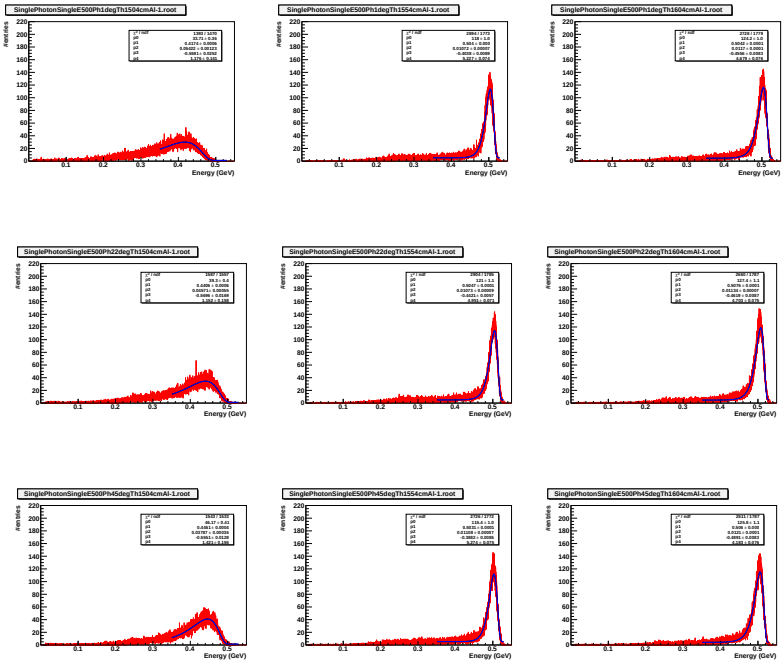

Figure 24: 500 MeV 4 cm Al

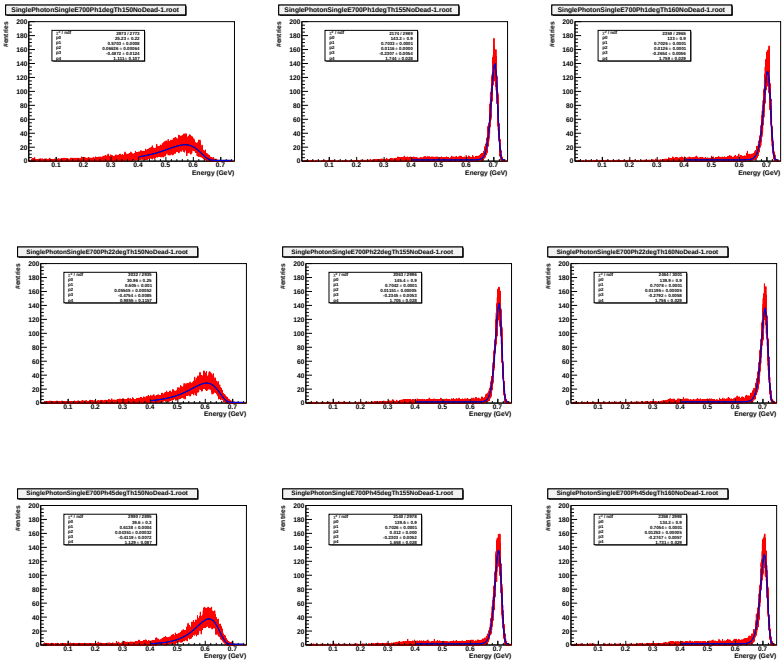

Figure 25: 700 MeV No dead material

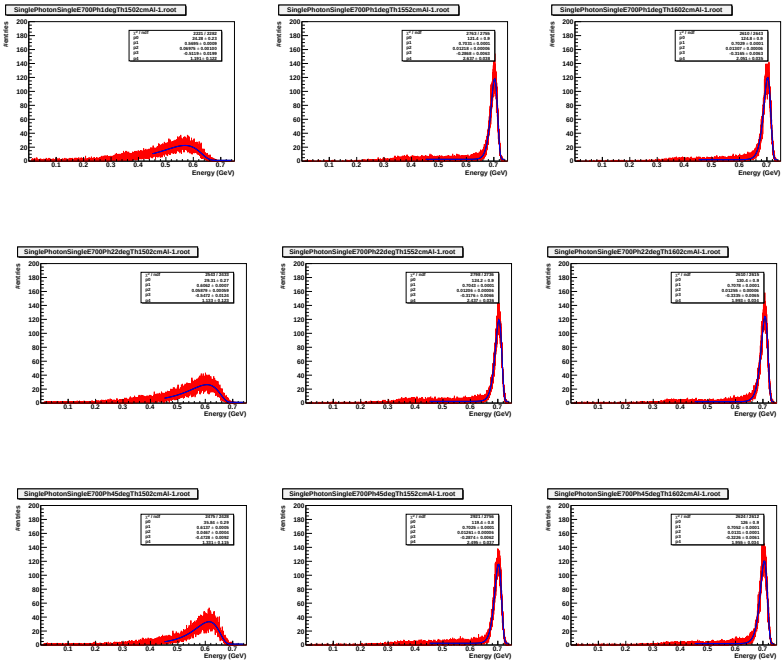

Figure 26: 700 MeV 2 cm Al

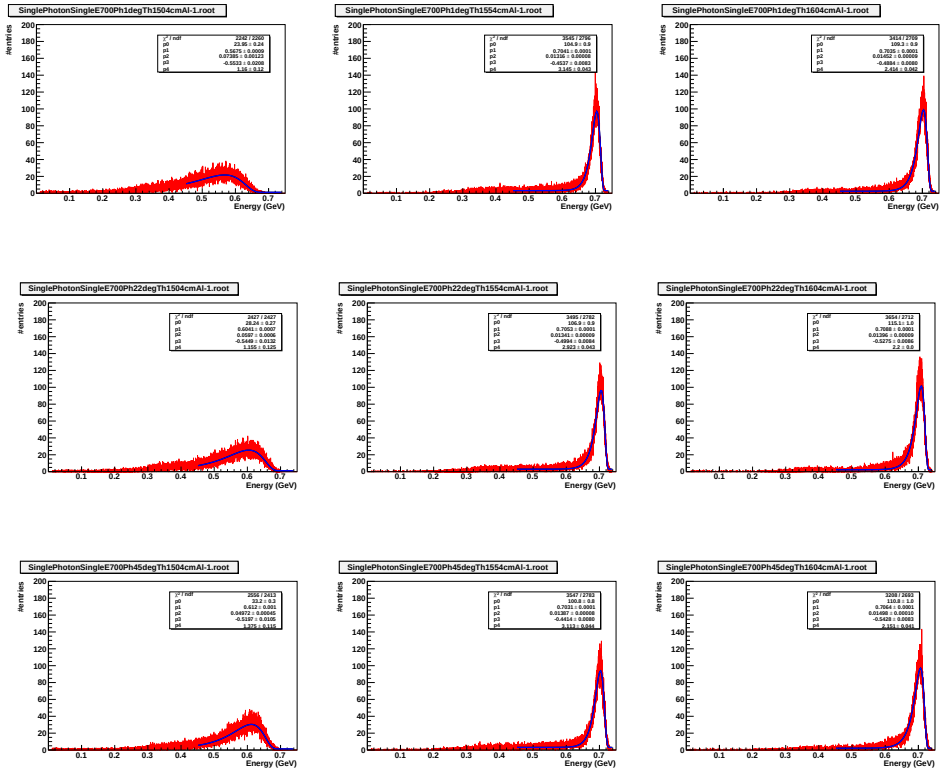

Figure 27: 700 MeV 4 cm Al

6.1.3 Histograms

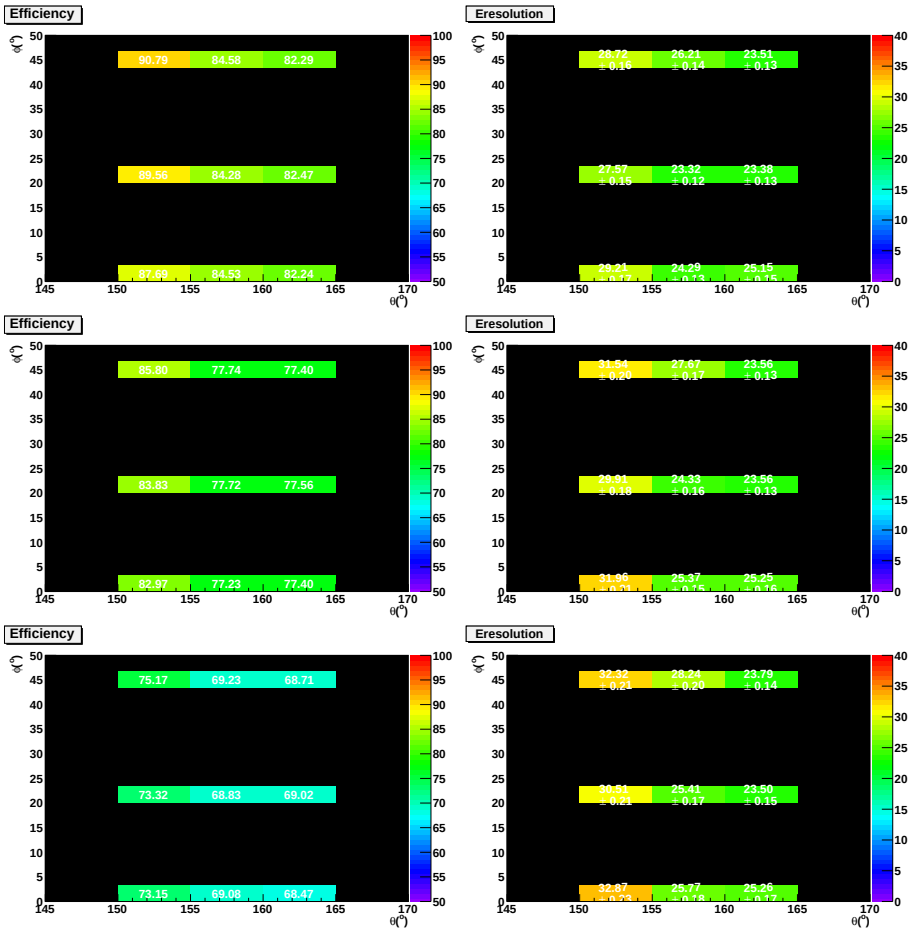

Figure 28: results for 30 MeV

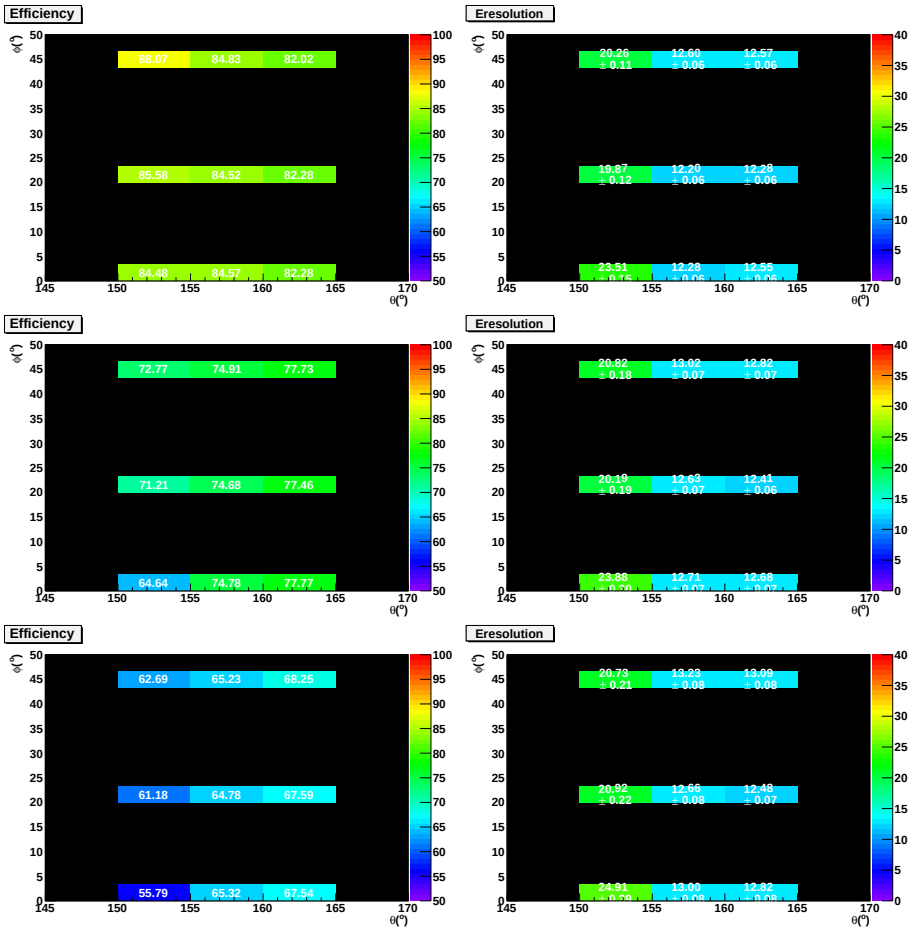

Figure 29: results for 100 MeV

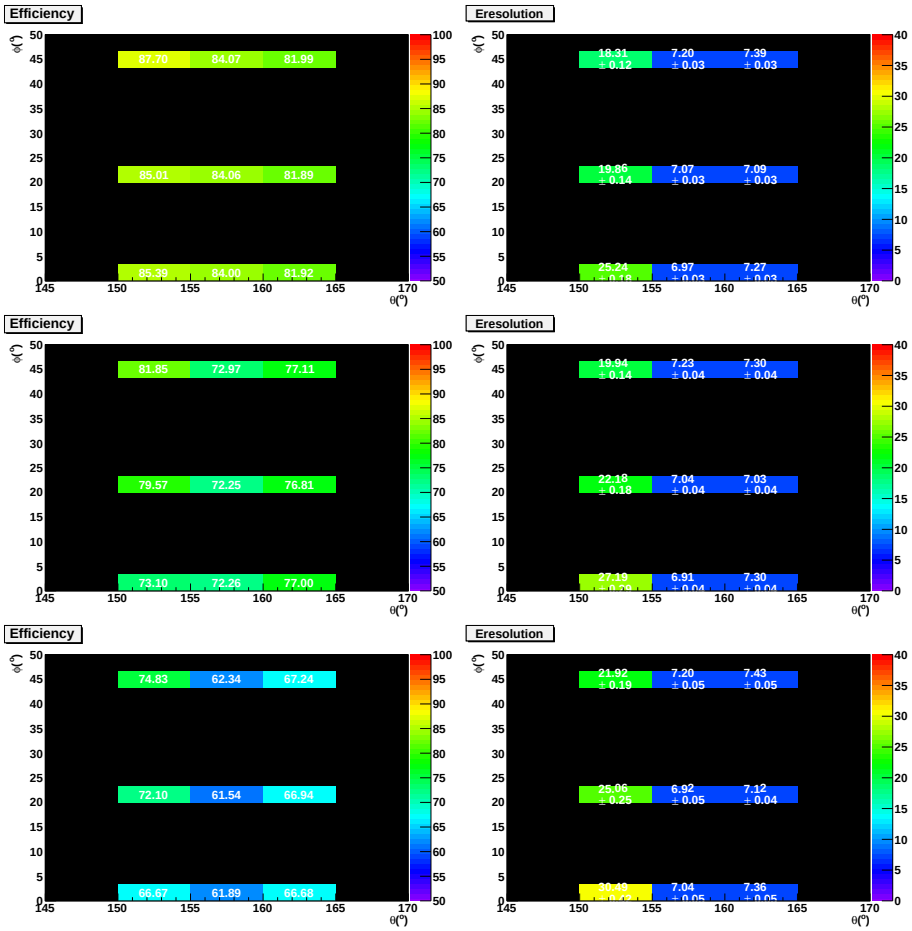

Figure 30: results for 250 MeV

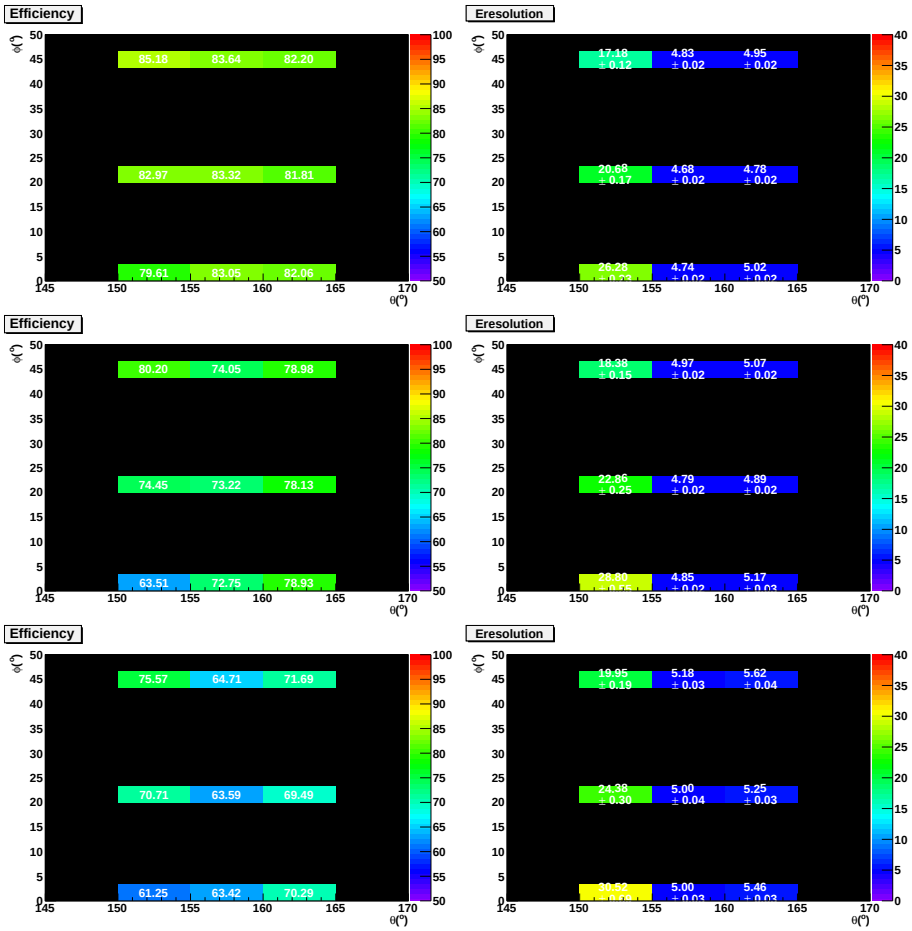

Figure 31: results for 500 MeV

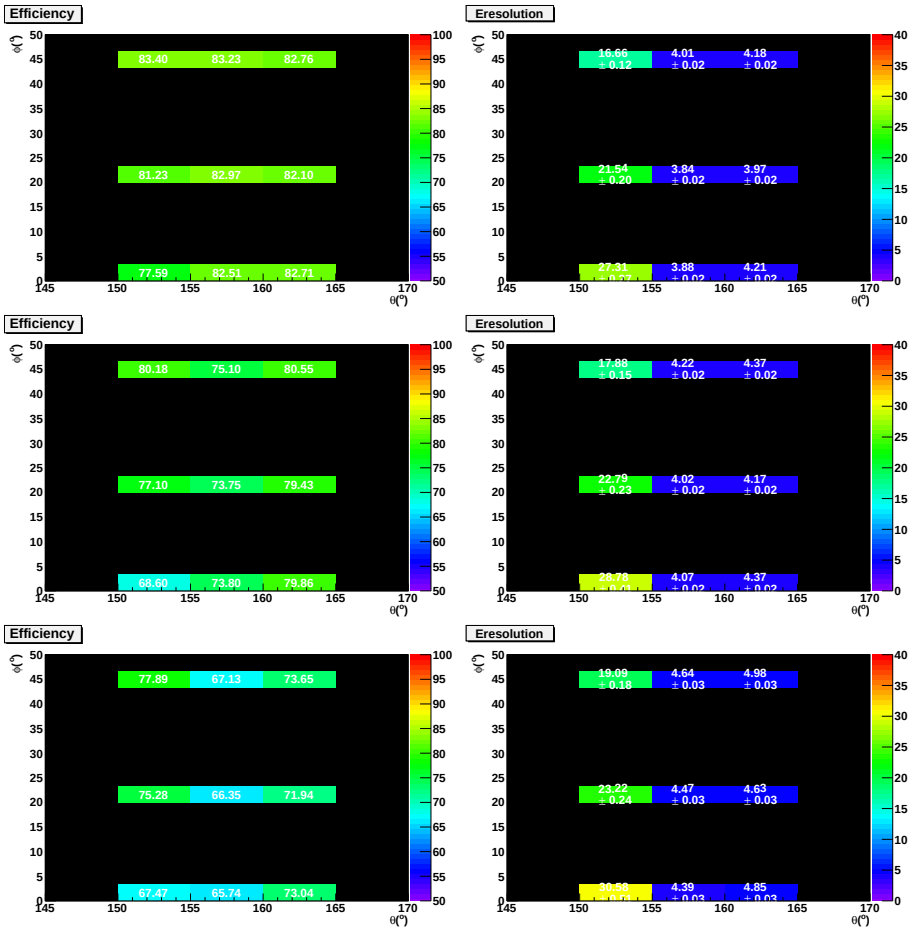

Figure 32: results for 700 MeV

6.2 Last simulation

6.2.1 Fits

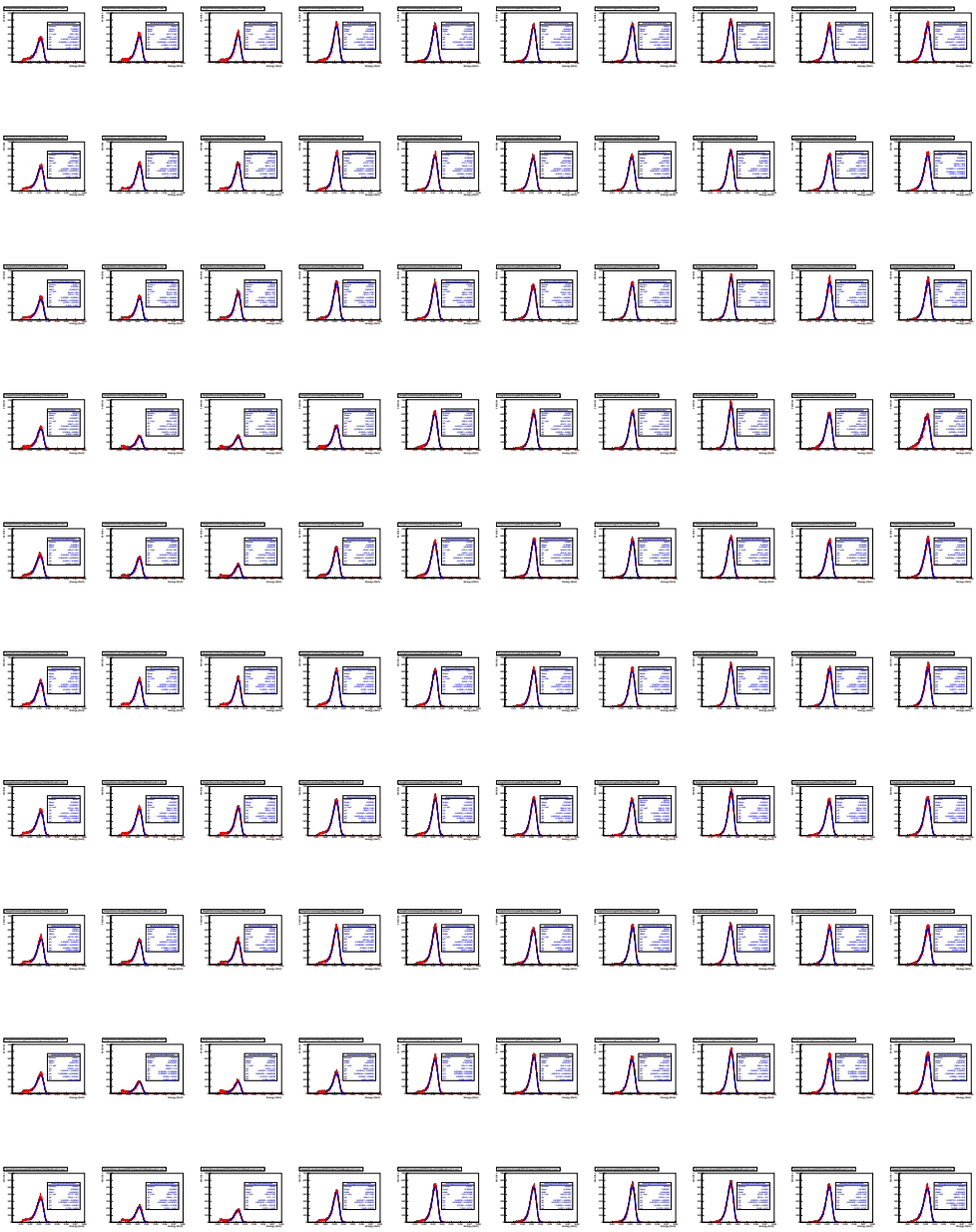

Figure 33: Histogram fits for 30 MeV case.

Figure 34: blablabla

Figure 35: jkslfhj

Figure 36: jklsdf

Figure 37: 700

6.2.2 Results

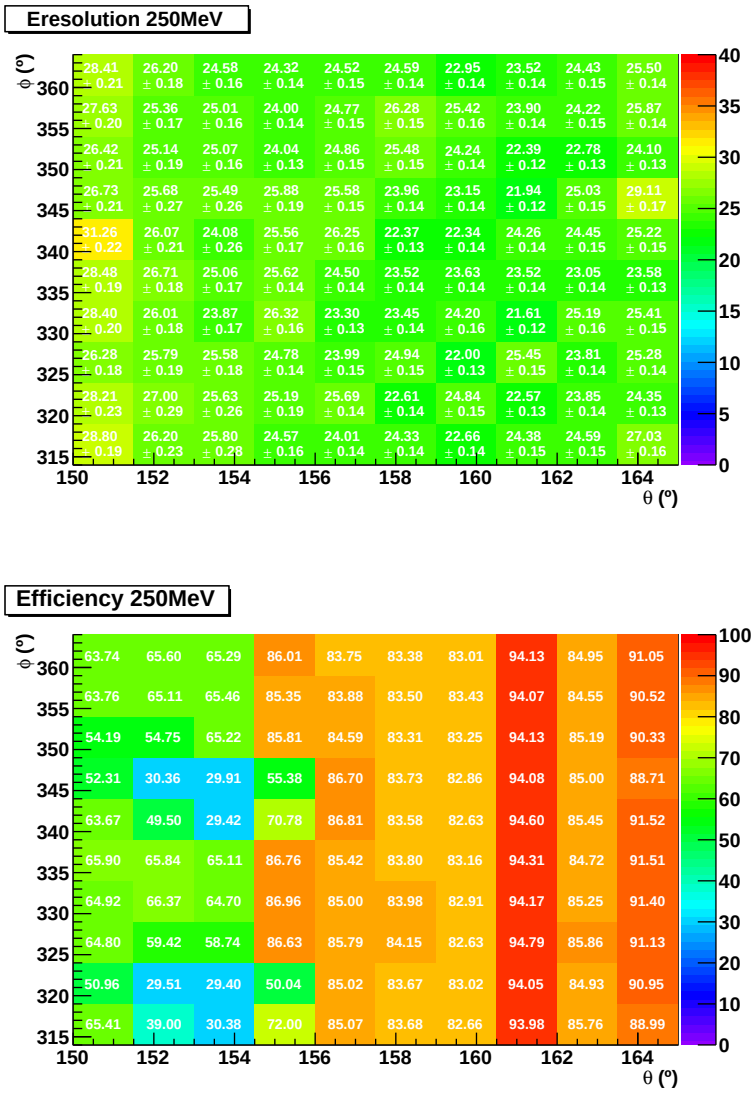

Figure 38: Energy resolution and Efficiency for 30 MeV case

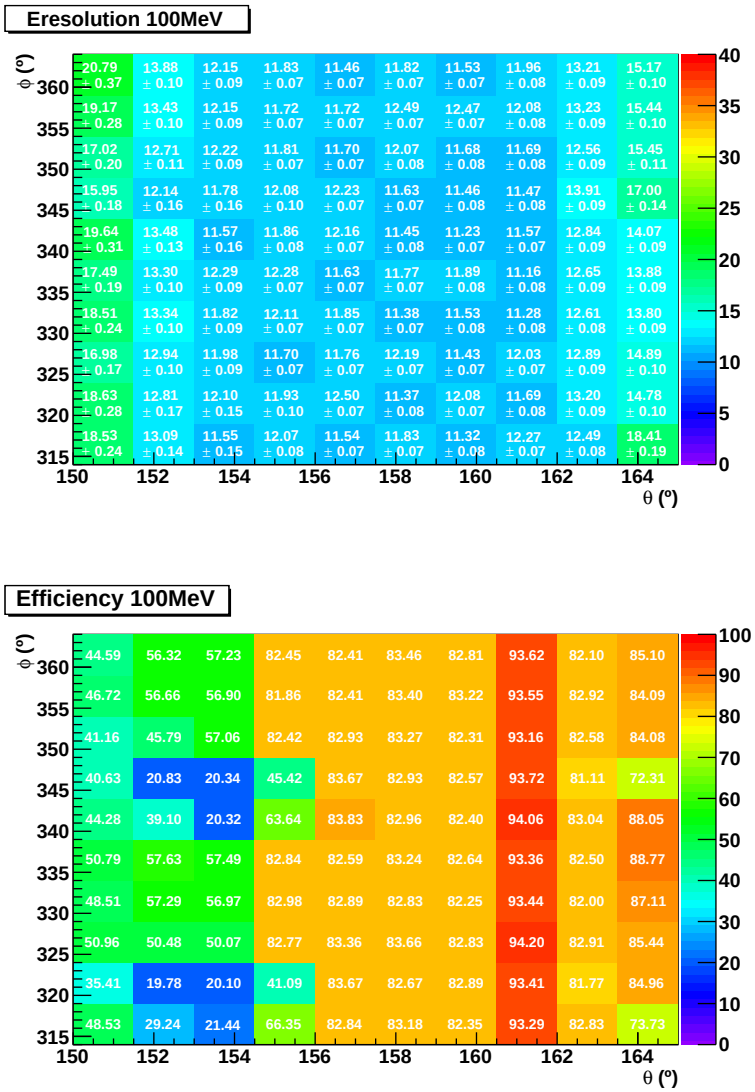

Figure 39: bblblblala

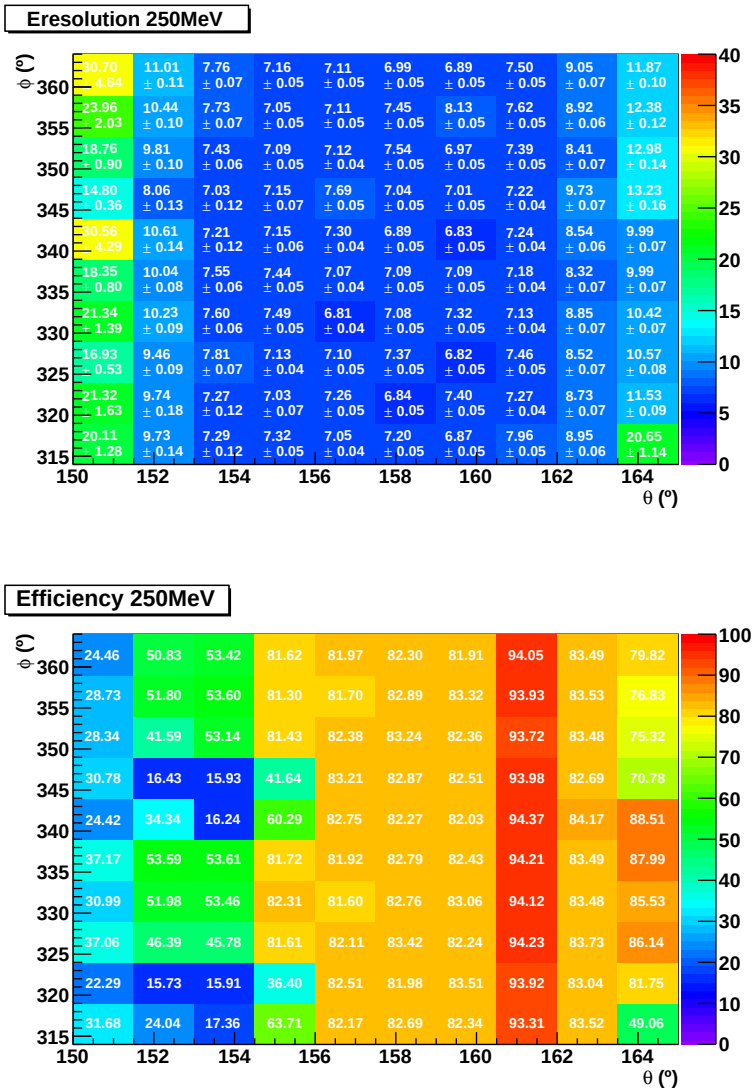

Figure 40: dlkjaksjdf

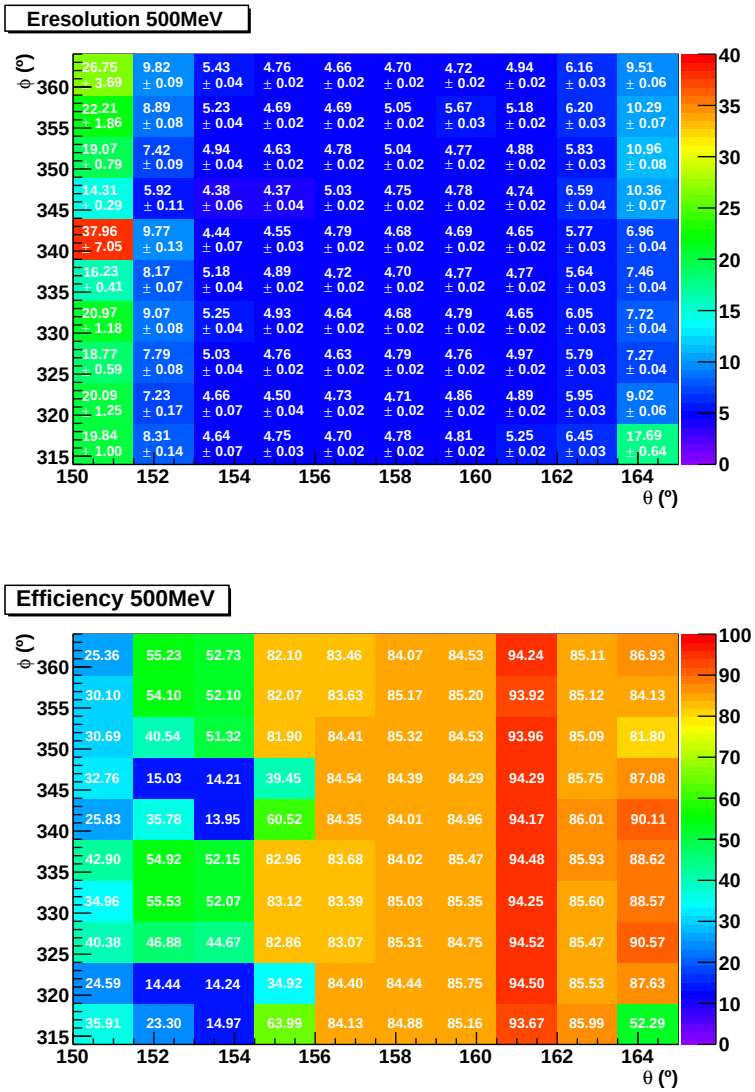

Figure 41: hjksa

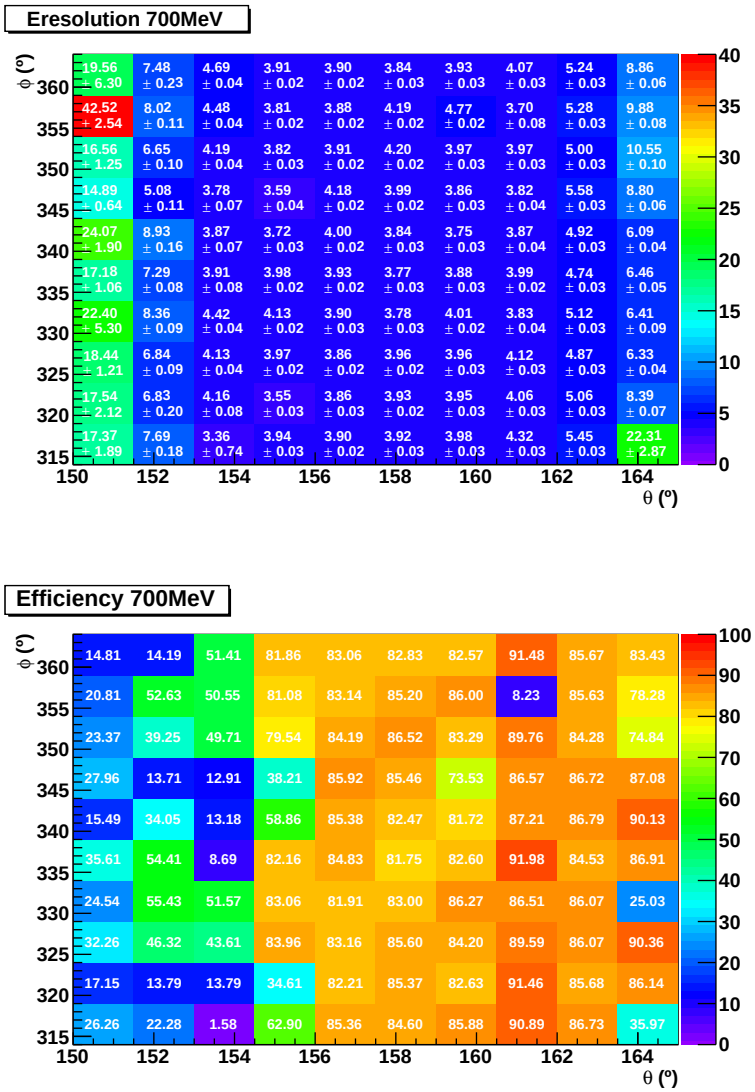

Figure 42: 700

References

[1] Feasibility studies of the time-like proton electromagnetic form factor measurement with P̄ANDA at FAIR. M. Sudol, M. C. Mora Espí et al.

[2] Testing axial and electromagnetic nucleon form factors in time-like regions in the processes $\bar{p}p \to \pi^- + l^- + l^+$ and $\bar{p} + p \to \pi^0 + l^- + l^+$, $l = e, \mu$. C. Adamuscin, E. A. Kuraev, E. Tomasi-Gustafsson and F. E. Maas.

[3] Antiproton-nucleus electromagnetic annihilation as a way to access the proton timelike form factors. H. Fontvieille and V. A. Karmanov.

[4] New possibility for further measurements of nucleon form factors at large momentum transfer in time-like region: $\bar{p} + p \to l^+ + l^-$, $l = e$ or μ. E. Tomasi-Gustafsson and M. P. Rekalo.

[5] talk at gsi, estimation of dead material for mvd.